Available online at www.sciencedirect.com
ScienceDirect
Journal of Nuclear Materials 373 (2008) 28–38
journal of nuclear materials
www.elsevier.com/locate/jnucmat

Influence of Cu, Cr and C on the irradiation defect in Fe: A molecular dynamics simulation study

Je-Wook Jang [a], Byeong-Joo Lee [a,*], Jun-Hwa Hong [b]

[a] Department of Materials Science and Engineering, Pohang University of Science and Technology, Pohang 790-784, Republic of Korea
[b] Nuclear Materials Technology R&D Team, Korea Atomic Energy Research Institute, Taejon 305-353, Republic of Korea

Received 3 November 2006; accepted 12 April 2007

Abstract

The effects of alloying elements, Cu, Cr and C, on the number of residual point defects (vacancies and interstitials), their clustering tendency and constitution have been investigated by performing molecular dynamics cascade simulations on pure Fe, Fe–0.5 at.% Cu, Fe–10 at.% Cr and Fe–0.1 at.% C alloys using MEAM interatomic potentials. Both Cu and Cr form Fe–M and M–M interstitial dumbbells, but have no significant effect on the number and clustering tendency of point defects. Carbon has no effect on the formation and clustering of point defects neither, but shows a strong binding with vacancies and interstitial dumbbells. By combining the simulation results and calculated binding energies between individual point defects, effects of solute atoms on the long-term irradiation-induced microstructure evolution are deduced. Details of cascade simulation results and binding energies between point defects are presented, and influence of solute elements on long-term irradiation defect such as void swelling and formation of solute-rich precipitates are discussed.
© 2007 Elsevier B.V. All rights reserved.

PACS: 31.15.Qg; 61.72.Cc; 61.72.Ji; 61.82.Bg

1. Introduction

Various defects are created by displacement cascades during heavy-ion and fast-neutron irradiation on structural components in nuclear reactors. The point defects created by cascades have effects on the microstructure changes, and eventually cause irradiation induced embrittlement, hardening and void swelling which are connected to the safety and life-time of nuclear structural steels. Therefore, it is important to carefully monitor and predict the microstructure evolution under long-term irradiation. Because of the difficulties in handling irradiated materials and in experimental examination of atomic scale structural changes, atomistic simulation approaches such as molecular dynamics (MD) have been used widely for the investigation of irradiation effects in nuclear structural materials [1–16].

For pure iron, extensive MD cascade simulations have been performed [1–8] mainly using the Finnis–Sinclair (FS) type interatomic potential developed by Calder and Bacon [1], and statistically meaningful information on the irradiation-induced primary defect formation is now available [6,8]. However, for application to actual nuclear structural steels, the effects of alloying and/or impurity elements such as Cu, Cr, Ni, Mn, Mo and C should be considered. Those alloying/impurity elements are expected to affect various irradiation damage related properties and it is necessary to carefully investigate the effects of individual elements on the irradiation defect formation. For example, copper is well known to cause embrittlement in nuclear reactor pressure vessel steels by forming Cu-rich precipitates [17,18]. Many cascade simulations have been carried out for Fe–Cu alloys [9–11] using different interatomic potentials, the FS type [19], EAM (embedded atom

* Corresponding author. Tel.: +82 54 279 2157; fax: +82 54 279 2399.
E-mail address: calphad@postech.ac.kr (B.-J. Lee).

0022-3115/$ - see front matter © 2007 Elsevier B.V. All rights reserved.
doi:10.1016/j.jnucmat.2007.04.046

method) [20] and the MEAM (modified EAM) [11]. Concerning the effect of Cu on the number of residual defects, all simulations show similar results. However, for the formation of Fe–Cu mixed dumbbells (as interstitial defect) and clustering tendency of primary defects, some potential dependencies have been observed [9–11]. Further, in the case of the MEAM simulation, more MD runs are necessary to obtain statistically more meaningful numerical results. In high-Cr ferritic/martensitic steels, which are attractive as structural materials for fusion reactors, it is known that the alloying element Cr certainly has an effect on hardening and swelling [21], but the detailed role of Cr is not fully understood. Even though cascade simulations have also been performed for the Fe–Cr alloys [12–16] using two different EAM [12,22] and FS type potentials [16], because of the potential dependency of the results, another simulation using different interatomic potential (for example, MEAM [23]) is highly recommended for comparison. Carbon is an essential element in steels and is expected to have a significant effect on microstructure evolution even in low concentrations through strong binding with primary defects [24–26]. Even though there is a strong need for the investigation of carbon effects on the irradiation defect formation, the Fe–C system has never been investigated by atomistic approaches because reliable interatomic potential for the Fe–C system has not been available.

With recent development of the MEAM interatomic potential for the Fe–C system [27], cascade simulations for carbon effects on irradiation defect formation are now feasible. Further, even though many cascade simulations were performed for pure Fe, Fe–Cu and Fe–Cr alloys as briefly reviewed in the above, it should be noted that different interatomic potentials have been used for pure Fe in simulations for individual systems. Because of the potential dependency of cascade simulation results, it would be meaningful to perform simulations for all the relevant alloy systems using the same (MEAM) Fe potential.

The purpose of the present work is to investigate the influence of Cu, Cr and C on the primary irradiation defect formation in Fe consistently by performing MD cascade simulations using the same MEAM potential for Fe. The number of residual defects, clustering tendency and binding between solute atoms and primary defects were examined. To rationalize the results of cascade simulations, various defect binding energies were calculated. In addition to the effects of solute elements on the irradiation defect formation during the primary stage of irradiation damage, based on the simulation and calculation results, the roles of the alloying elements on the microstructure evolution during long-term irradiation such as precipitation or void swelling were discussed.

2. Simulation method

The interatomic potentials used in the present work are the second-nearest-neighbor (2NN) MEAM type developed by Lee and Baskes [28,29] by modifying the MEAM potential formalism originally developed by Baskes [30]. The details of the potentials are documented elsewhere for Fe [29], Fe–Cu [11], Fe–Cr [23] and Fe–C [27]. The 2NN MEAM formalism includes up to second-nearest-neighbor interactions. Therefore, the radial cutoff distance during atomistic simulations should be at least larger than the second-nearest-neighbor distance in structures under consideration. All calculations presented here are those performed with a radial cutoff distance (3.6 Å) whose size is between the second- and third-nearest-neighbor distances of bcc Fe.

Molecular dynamics simulations of displacement cascades are performed using a constant pressure periodic boundary condition based on the Parinello–Rahman method [31] with a Verlet algorithm [32]. A block of atoms is first equilibrated at a given temperature for at least 10 ps. Then, an atom is given a velocity that corresponds to a given kinetic energy (MD cascade energy or PKA energy) in a specific direction so that a cascade is started. According to the MEAM potential, the distance between two atoms that form an equilibrium $\langle 1\,1\,0\rangle$ dumbbell in bcc Fe corresponds to $0.724a$ at 0 K, where a is the lattice parameter. This is very close to the value $0.725a$ obtained by Calder and Bacon [1] using their FS type potential. Therefore, following the scheme by Calder and Bacon, when counting the number of primary defects in the present work, a lattice site with no atom within a distance of $0.3a$ is counted as a vacancy and an atom that deviates more than $0.3a$ from a lattice site is counted as an interstitial atom. The standard output of cascade simulation includes the total number of residual vacancies and interstitials at the end of cascade cooling phase, the fraction of vacancies and interstitials forming clusters, and the size distribution and constitution of these primary defects.

In the present work, cascade simulations were performed for pure Fe and Fe-based binary alloys with 0.5 at.% Cu, 10 at.% Cr or 0.1 at.% C. 10 at.% is a typical Cr content in high Cr ferritic/martensitic steels. 0.5 at.% Cu and 0.1 at.% C are a little bit higher compared to typical concentrations of individual elements in nuclear structural steels, but were chosen to see the alloying effect more clearly. The PKA energy and the temperature were 2 keV and 573 K, respectively. Even though the PKA energy of 2 keV is rather small compared to the values used in other cascade simulation studies (~50 keV), no significant change of clustering tendency of vacancies or interstitials is reported above this PKA energy value [4]. Therefore, it is thought that meaningful results would be obtained for the clustering tendency of primary defects and effects of alloying elements on it in various systems (pure Fe and binary alloys) using the 2 keV.

The number of atoms involved in each simulation was 54 000 ($30 \times 30 \times 30$ unit cells). It is believed that the simulation box size effect is negligible as far as the box size is large enough not to allow the overlapping of cascade region due to the periodic boundary condition. As

representative PKA directions for an average behavior, both ⟨1 3 5⟩ and ⟨2 3 5⟩ were selected. Several MD runs (14 for Fe, 13 for Fe–Cu, 14 for Fe–Cr, and 8 for Fe–C) were performed by changing equilibration time, location of PKA atom and PKA direction to achieve statistically representative results. Though the initial equilibration temperature was 573 K, the final temperatures were around 700 K at the end of cascade simulations. A few simulations were also performed at 100 K for pure Fe for comparison with 573 K results and to estimate the temperature effect. It should be mentioned here that a few cascade simulations have been performed previously by the present authors for pure Fe and Fe–0.5 at.% Cu alloys using the same interatomic potentials and at the same conditions (PKA energy and temperature). The previous results [11] were included in the present work when analyzing the simulation results.

3. Results of cascade simulations

The changes in the number of defects as a function of time were similar in all the cascade simulations for pure Fe and Fe-based binary alloys. The peak time in the number of defects was around 0.3 ps. After 5 ps no significant change was detected. Fig. 1 presents configurations of point defects at the end of cascade simulations (10 ps) in pure Fe and alloys. White spheres represent vacancies, while gray (or green) and black (or red) spheres represent interstitial Fe and interstitial solute atoms, respectively. Notice that all solute carbon atoms are visible in the Fe–C alloy (Fig. 1(d)) even though they are not counted as interstitial defects. As shown in Fig. 1, the alloying elements Cu, Cr and C do not give a significant effect on the residual number of defects and their spatial distribution during the primary stage of irradiation damage.

To see the number and size distribution (or clustering tendency) of residual defects and effects of alloying elements on them, more quantitative analyses of the residual defects were carried out. Table 1 shows the total number of vacancies and interstitials, the number of single defect, di- or tri-defect clusters, and the fraction of defects forming clusters in the four material systems: pure Fe, Fe–Cu, Fe–Cr and Fe–C alloys, at the end of 10 ps cascade simulations. When single defects are located within second-nearest-neighbor distance from each other, they are counted as a defect cluster. In Table 1, '2V', '3V', '2I' and '3I' mean di-, tri-vacancy clusters, di- and tri-interstitial clusters, respectively. The present results show that for the 2 keV and 573 K cascade, approximately 10% of the residual vacancies and 30% of interstitials form clusters. At low temperature (100 K), the number of residual defects does not change significantly but the clustering tendency both of vacancies and interstitial defects decreases. The effect

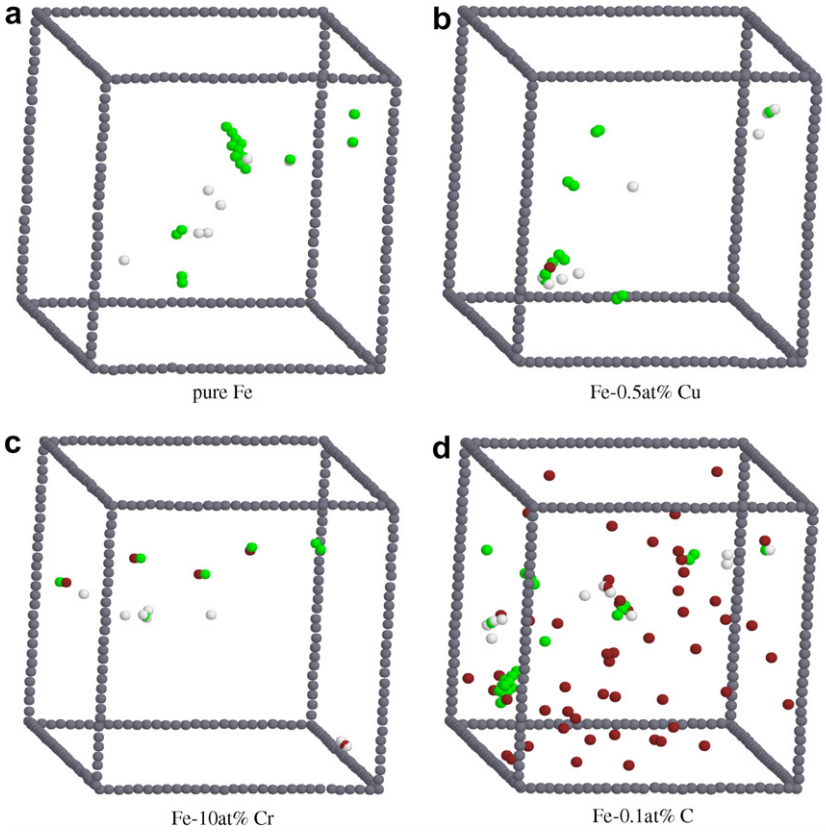

Fig. 1. Configurations of residual point defects at the end of cascade simulations (10 ps) with a PKA energy of 2 keV at 573 K. White spheres represent vacancies, the gray (or green in the web version) spheres represent interstitial Fe atoms and the black (or red in the web version) spheres represent interstitial solute atoms.

Table 1
The number and size distribution of residual defects and defect clusters in pure Fe and Fe–0.5 at.% Cu, Fe–10 at.% Cr and Fe–0.1 at.% C alloys with a PKA energy of 2 keV at 573 K

	Total vacancy	Single vacancy	Total interstitial	Single interstitial	2V	3V	2I	3I	Fraction of V in clusters	Fraction of I in clusters
Fe, total in 6 MD runs at 100 K										
Average (STDEV)	5.83 (2.11)	5.83 (2.11)	5.83 (2.11)	4.67 (2.13)	0/6	0/6	2/6	1/6	0.00	0.20
Fe, total in 14 MD runs at 573 K										
Average (STDEV)	6.00 (1.85)	5.43 (1.84)	6.00 (1.85)	4.07 (2.02)	4/14	0/14	9/14	3/14	0.10	0.32
Fe–Cu, total in 13 MD runs at 573 K										
Average (STDEV)	5.77 (1.42)	5.31 (1.59)	5.77 (1.42)	3.92 (1.73)	3/13	0/13	9/13	2/13	0.08	0.32
Fe–Cr, total in 14 MD runs at 573 K										
Average (STDEV)	6.64 (2.06)	6.00 (1.96)	6.64 (2.06)	4.86 (1.68)	3/14	1/14	8/14	3/14	0.10	0.27
Fe–C, total in 8 MD runs at 573 K										
Average (STDEV)	6.00 (1.12)	5.25 (1.30)	6.00 (1.12)	4.38 (1.87)	3/8	0/8	5/8	1/8	0.13	0.27

Two or more single defects located within second-nearest-neighbor distance from each other are counted as a defect cluster. 2V and 3V mean di- and tri-vacancy clusters, while 2I and 3I mean di- and tri-interstitial clusters, respectively.

of alloying elements on the total number, clustering tendency and size distribution of residual defects looks not significant.

Even though the solute atoms do not have significant effect on the number or clustering of residual defects, they do have a certain effect on the constitution of residual defects. According to the present analysis (Table 2), approximately 10% and 69% of interstitial defects (dumbbell or crowdion) involve a solute atom in the Fe–0.5 at.% Cu and Fe–10 at.% Cr alloys, respectively. Carbon atoms cannot be a component of interstitial defects, but the present analysis shows that approximately 27% of interstitials are bound by carbon atoms. Although the numeric value is smaller than the case of interstitials, high percentage (4%) of vacancies are also bound by carbon atoms in the Fe–0.1 at.% C alloys.

Both Cu and Cr are elements that cause Cu-rich or Cr-rich precipitations, which affect the mechanical property of steels. The irradiation would certainly enhance the diffusion of solute atoms and the above-mentioned precipitations. Generally the vacancy mechanism is accepted as the main mechanism for diffusion of substitutional atoms in metals. However, because equal amount of interstitial defects are also created during irradiation and because interstitials have higher mobility than vacancies, there exists a possibility that the interstitial mechanism can be an important additional mechanism of diffusion. To evaluate the possibility of interstitial mechanism of diffusion for substitutional solute atoms (Cu and Cr) and effect of the interstitial carbon atoms on such diffusivity, the fraction of solute atoms within the second- and third-nearest-neighbor distances of all individual defects (solute atoms, interstitials and vacancies) were examined. The results are listed in Table 3. Here, the data on the first row in each item are for second-nearest-neighbor distance while those on the second row are for third-nearest-neighbor distance.

Out of 54 000 atoms in a simulation block, the number of Cu atoms is 265 or 273 (0.5%). Initially, the average fraction of Cu within second- and third-nearest-neighbor distance of individual Cu atoms is 0.43% and 0.44%, respectively. After cascade simulations, the fraction becomes 0.44% and 0.46%, respectively. The increase cannot be considered statistically significant. This means that during the 10 ps cascade evolution, the amount of additional Cu–Cu clustering is negligible. The same results are obtained also for Cr–Cr or C–C clustering. Further, the fractions of individual solute atoms around vacancies are not much different from the overall fractions except carbon which is about twice of what expected from the overall fraction. However, the situation is different if neighbors of interstitials are considered. In all the binary alloys considered, the fraction of solute atoms within the second- and third-nearest-neighbor distance from the individual interstitials is significantly higher than the average values of individual solute elements. The formation of Fe–Cu or Fe–Cr mixed dumbbells and the high population of solute

Table 2
Percentage of primary defects involving solute atoms or bound by carbon atoms

# of interstitial Cu atoms/# of total interstitials in Fe–0.5 at.% Cu alloys	7% (0.38/5.77)
# of interstitial Cr atoms/# of total interstitials in Fe–10 at.% Cr alloys	69% (4.57/6.64)
Percentage of interstitials bound by carbon atoms in Fe–0.1 at.% C alloys	27% (1.63/6.00)
Percentage of vacancies bound by carbon atoms in Fe–0.1 at.% C alloys	4% (0.25/6.00)

Table 3
Distribution of component atoms within second- and third-nearest-neighbor distances of individual defects in Fe–0.5 at.% Cu, Fe–10 at.% Cr and Fe–0.1 at.% C alloys

	Fe atoms	Cu atoms	Total (mean)	Fraction of Cu (%)
Fe–0.5 at.% Cu				
Around 265 × 2, 273 × 2 Cu atoms	14428	62	14490 (13.5)	0.43
Before cascade simulation (4 sets)	27182	120	27302 (25.4)	0.44
Around 265 × 6, 273 × 7 Cu atoms	47016	210	47226 (13.5)	0.44
After cascade simulation (13 sets)	88777	408	89185 (25.5)	0.46
Around 75 interstitials	2680	19	2699 (36.0)	0.70
After cascade simulation (13 sets)	5994	41	6035 (80.5)	0.68
Around 75 vacancies	1364	5	1369 (18.3)	0.37
After cascade simulation (13 sets)	2539	14	2553 (34.0)	0.55
				Fraction of Cr (%)
Fe–10 at.% Cr				
Around 5344 × 2 Cr atoms	128832	14304	143136 (13.4)	9.99
Before cascade simulation (2 sets)	240437	26568	267005 (25.0)	9.95
Around 5344 × 14 Cr atoms	902018	100240	1002258 (13.4)	10.0
After cascade simulation (14 sets)	1694689	187704	1882393 (25.2)	9.97
Around 93 interstitials	2332	366	2698 (29.0)	13.6
After cascade simulation (14 sets)	5434	710	6144 (66.1)	11.6
Around 93 vacancies	1567	189	1756 (18.9)	10.8
After cascade simulation (14 sets)	2912	326	3238 (34.8)	10.1
				Fraction of C (%)
Fe–0.1 at.% C				
Around 54 × 2 C atoms	1710	4	1714 (15.9)	0.23
Before cascade simulation (2 sets)	3490	4	3494 (32.4)	0.11
Around 54 × 8 C atoms	6731	14	6745 (15.6)	0.21
After cascade simulation (8 sets)	13792	14	13806 (32.0)	0.10
Around 48 interstitials	1707	23	1730 (36.0)	1.33
After cascade simulation (8 sets)	3785	32	3817 (79.5)	0.84
Around 48 vacancies	856	2	858 (17.9)	0.23
After cascade simulation (8 sets)	1601	2	1603 (33.4)	0.12

For each alloy, the data in the first item are for the initial samples before cascade simulations and the others are for the given number of samples after cascade simulations. For each item the data on the first row are for second-nearest-neighbor distance while those on the second row are for third-nearest-neighbor distance.

atoms around the interstitial dumbbells indicates that the diffusion of substitutional solute atoms (Cu and Cr) can be further enhanced by the interstitial mechanism. On the other hands, the strong binding between interstitial dumbbells and carbon atoms is expected to play a role in a way to retard the diffusion of substitutional atoms by the interstitial mechanism because the mobility of interstitial carbon atom is much lower than those of interstitial dumbbells as will be discussed in the next section.

4. Discussion

The present cascade simulations show that the number of residual primary defects and their clustering tendency are hardly affected by solute atoms, Cu, Cr and C, during the single displacement cascade with a PKA energy of 2 keV. However, the effect of Cu on the irradiation induced embrittlement [17,18] and that of Cr on the void swelling [21] are well established experimental facts. The strong binding between vacancy and a carbon atom, which will have effect on the clustering of vacancies, is also experimentally well established [24–26]. The reason for the discrepancy between the simulation and experimental observations should certainly be the low PKA energy of 2 keV and the short simulation time of 10 ps. However, other simulations on the Fe–Cu [9,10] and Fe–Cr [13–16] alloys report the same conclusions even at higher PKA energy up to 50 keV and longer simulation time up to 40 ps. This means that the MD simulation time, several tens of picoseconds, is too short to see any meaningful structural evolutions. In the present section, a rationalization of the simulation results will be attempted by calculating binding energies between various individual defects. Based on the calculations, an attempt will also be made to presume the effect of solute atoms on the long-term structural evolution.

In addition to the number of residual defects and clustering tendency, what is first observed in the present study is that the clustering tendency of interstitial defects is larger than that of vacancies. As shown in Table 1, about 30% of interstitials form clusters while about 10% of vacancies do. This difference can be explained by comparing the size of binding energies between two vacancies and between two interstitials. The binding energy between two defects is

Table 4
Calculated binding energies between vacancies and between interstitial dumbbells in bcc Fe, and effect of solute atoms on the bindings (eV)

	Fe	Fe–Cu	Fe–Cr	Fe–C
Vac–Vac (1NN/2NN)	−0.13/0.02 0.06/0.15[a] 0.16/0.21[b], 0.14/0.19[c]	−0.006/0.15	−0.12/0.06	−0.04/0.67
$\langle 1\,1\,1\rangle_{FeFe} - \langle 1\,1\,1\rangle_{FeM}$	1.486 1.37[d]	1.439	1.434	1.381[e]

1NN and 2NN means the vacancies are first-nearest-neighboring and second-nearest-neighboring from each other, respectively. The effect of solute atoms represents the case where a solute atom is present as a nearest neighbor to the di-vacancy cluster or a component of the interstitial dumbbell. For each item, the data on the first row are from the present calculation and others are from other calculations.

[a] Ref. [33] (First principles).
[b] Ref. [10,20] (Empirical potential).
[c] Ref. [19] (Empirical potential).
[d] Ref. [34] (First principles).
[e] The most stable configuration of the dumbbell–carbon–dumbbell cluster is the nearest neighboring parallel $\langle 1\,1\,0\rangle$ dumbbells and a carbon atom on the nearest neighboring octahedral site. (see Fig. 2).

defined as the energy gained as they approach to the first or second-nearest-neighbor distance from an infinite distance. The binding energies between two vacancies and two interstitial dumbbells in pure Fe and when a solute atom presents as a nearest neighbor to the vacancy cluster or when a solute atom is a component of interstitial dumbbells are presented in Table 4. According to the present calculation, $\langle 1\,1\,1\rangle$ dumbbells are more stable when interstitials are clustered, while $\langle 1\,1\,0\rangle$ dumbbells are more stable for a single interstitial dumbbell in pure Fe, Fe–Cu and Fe–Cr alloys. However, the opposite occurs when a carbon atom is neighboring the dumbbell–dumbbell cluster. The most stable configurations of dumbbell–dumbbell clusters in individual systems are illustrated in Fig. 2. As shown in Table 4, the binding energy between interstitial dumbbells is much larger than that between two vacancies. The large binding energy and relatively high mobility of interstitial dumbbells are thought to be the reason for the larger clustering fraction of interstitials shown in Table 1. Recent two simulation studies [15,16] on pure Fe and Fe–Cr alloys using two different potentials show that the clustering fraction of interstitials is slightly higher than 30% at the same PKA energy level, in good agreement with the present study. In the case of clustering fraction of vacancies, the EAM simulation [15] shows higher values (20–27%) while the FS simulation [16] shows comparable values (5–20%). The FS potential by Calder and Bacon [1], which has been used most widely for the cascade simulation of pure Fe, gives about 25% and 50% for the clustering fraction of vacancies and interstitial defects, respectively [4]. Even though there are some potential dependencies in clustering fractions, all simulations show that the clustering tendency of interstitials is generally higher than that of vacancies.

The second observation in the present simulation is the formation of Fe–M mixed and even M–M foreign interstitial dumbbells both in the Fe–Cu and Fe–Cr alloys. The formation of mixed and foreign dumbbells implies a positive binding between an Fe–Fe self-interstitial dumbbell and a solute atom. The calculated binding energies of various dumbbells are presented in Table 5. Here, the reference states of individual bindings are an Fe–Fe self-interstitial dumbbell of given direction and a non-interacting solute atom. As expected, the mixed and foreign dumbbells have strong binding energies in both the Fe–Cu and Fe–Cr alloys. Within the framework of the MEAM (with many-body screening), the mixed dumbbell is a configuration where the interaction between a Cu or Cr atom and neighboring Fe atoms becomes minimal. Due to the positive

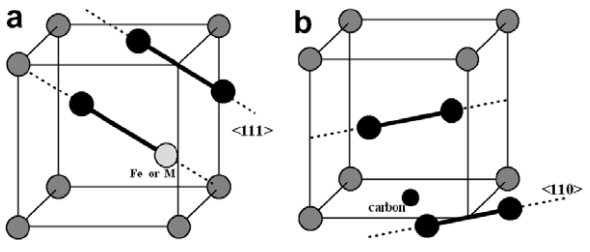

Fig. 2. The most stable configuration of a dumbbell–dumbbell cluster (a) in pure Fe, Fe–Cr and Fe–Cu alloys and (b) in Fe–C alloys with a neighboring carbon atom. Large spheres represent substitutional atoms while the small sphere represents a carbon atom. The large light gray atom (marked 'Fe or M') represents an interstitial Fe atom in pure Fe and an interstitial solute atom in Fe–Cr or Fe–Cu alloys.

Table 5
Calculated binding energies of $\langle 1\,1\,0\rangle$ and $\langle 1\,1\,1\rangle$ mixed or foreign interstitial dumbbells

	$\langle 1\,1\,0\rangle I_{FeM}$	$\langle 1\,1\,1\rangle I_{FeM}$	$\langle 1\,1\,0\rangle I_{MM}$	$\langle 1\,1\,1\rangle I_{MM}$
Fe–Cu	0.17 −0.22[a], −0.199[b]	0.23 0.2[a]	0.61	0.76
Fe–Cr	0.28 0.27[c], 0.10[d]	0.12 0.33[c], 0.20[d]	0.69 0.48[c]	0.27 0.46[c]

The reference states of individual bindings are an Fe–Fe self-interstitial dumbbell of a given direction and non-interacting solute atoms. For each item, the data on the first row are from the present calculation and others are from experiments or other calculations.

[a] Ref. [33] (First principles).
[b] Ref. [19] (Empirical potential).
[c] Ref. [15] (Empirical potential).
[d] Ref. [16] (Empirical potential, set II).

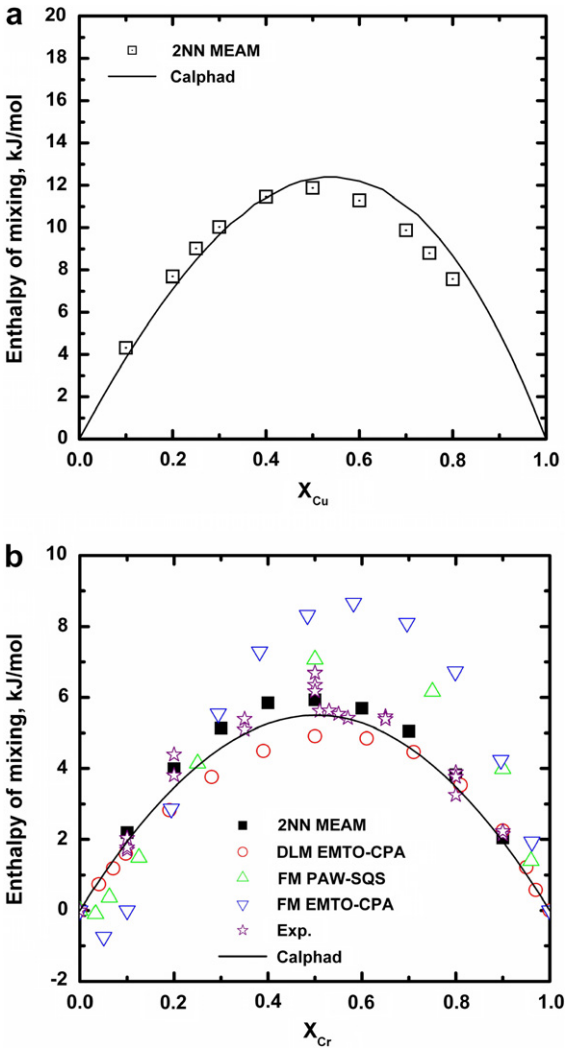

Fig. 3. Enthalpy of mixing of the (a) fcc Fe–Cu and (b) bcc Fe–Cr alloys, in comparison with experimental data [35], first principles calculations [36,37] and calphad thermodynamic calculations [38,39].

enthalpy of mixing between Fe and Cu or Cr atoms (Fig. 3), lowest energy is obtained when the Cu or Cr–Fe interaction becomes minimal. The large binding energies and again the relatively high mobility of interstitials are thought to be the reason for the high percentage of solute atoms in interstitial dumbbells as shown in Table 2. For the Fe–Cu alloys, none of the previous simulation studies [9,10] had reported the formation of mixed dumbbells even though it has been experimentally deduced [40]. The present simulation confirms the formation of mixed and even foreign dumbbells in the Fe–Cu alloys, first reported by the previous MEAM simulation [11]. For the Fe–Cr alloys, all simulation studies [13–16] report large amount of Fe–Cr and Cr–Cr interstitial dumbbells, in agreement with experiments [41–43]. According to the present Fe potential a $\langle 1\,1\,1\rangle$FeFe dumbbell has higher energy than a $\langle 1\,1\,0\rangle$FeFe dumbbell by 0.12 eV. In Table 5, the binding energy of $\langle 1\,1\,1\rangle$FeCu dumbbell is higher than that of $\langle 1\,1\,0\rangle$FeCu dumbbell and this makes the $\langle 1\,1\,1\rangle$FeCu dumbbell look more stable than the $\langle 1\,1\,0\rangle$FeCu dumbbell. However, this is because the reference states are different for the two binding energies. If the same $\langle 1\,1\,0\rangle$FeFe dumbbell is used for the reference state, the binding energy of $\langle 1\,1\,1\rangle$FeCu dumbbell becomes 0.11 eV which is smaller than that of $\langle 1\,1\,0\rangle$FeCu dumbbell, 0.17 eV.

Concerning the carbon, what is observed in the present simulation is the strong binding between a carbon atom and vacancies or interstitial dumbbells (Table 2). Actually, interstitial dumbbells show strong interactions with all kinds of solute atoms considered in the present study as shown in Table 3. In order to rationalize these observations, the interaction (binding) between individual primary defects and solute atoms were calculated and are shown in Table 6. As expected, carbon atoms have strong binding energies with all the vacancy, interstitial dumbbell and another carbon atom. The most stable configurations of carbon–carbon interaction and dumbbell–carbon binding are illustrated in Fig. 4, in comparison with first principles predictions [50]. What should be pointed out here is that the strongest binding is obtained for the vacancy–carbon binding although interstitial dumbbell–carbon binding is more frequently observed during the cascade simulations. This is thought to be because of the relatively higher mobility of interstitial dumbbells than vacancies.

To confirm the higher mobility of interstitials, migration energy barrier of vacancies and interstitials need to be calculated and compared to each other. The energy difference between $\langle 1\,1\,0\rangle$ and $\langle 1\,1\,1\rangle$ dumbbells has been used to estimate the migration energy barrier of interstitial dumbbells before a recent first principles calculation [34] proposes that the dominant migration mechanism for interstitial dumbbells may be translation-rotation jumps. In Table 7, the migration energy barriers of various interstitial dumbbells calculated based on the two approaches are presented. Migration energy barriers of Fe, Cu and Cr atoms by the vacancy mechanism and that of carbon atom by its own interstitial mechanism are also compared in Table 7. It is shown that the migration energy barriers of interstitial dumbbells are generally much lower than those of normal solute atoms. With lower migration energy barriers, relatively higher mobility of interstitial dumbbells can be easily expected. This must be the reason for why the interstitial dumbbell–solute atom bindings are observed more frequently during cascade simulations (Table 3) even though their binding energy values are comparable with those of other defect–solute atom bindings.

One more point that should be noticed in Table 7 is that the solute carbon atom has the highest migration energy barrier among all kinds of primary defects. The strong binding between vacancies or interstitial dumbbells and carbon atoms and the lowest mobility of solute carbon atoms indicate that the soluble carbon can play a role in a way to retard the diffusion and clustering of vacancies or interstitials, and hence retard the microstructure evolution during long-term irradiation. Actually such effect of soluble carbon would be small because most of carbon

Table 6
Calculated binding energies between a solute atom and individual point defects, a vacancy, a self-interstitial dumbbell and a solute atom

	Fe–Cu	Fe–Cr	Fe–C
M–Vac (1NN/2NN)	0.098/0.103	0.01/−0.00	0.90
	0.14[a], 0.11/0.10[b]	0.17/0.20[e]	0.41[h], 0.85[i], 1.05[j], 1.1[k]
	0.19/−0.03[c], 0.087/0.04[d]	0.035/−[f], −0.002/−0.01[g]	0.44[l], 0.41[m], 0.48[n]
M–$\langle 110\rangle I_{FeFe}$[o]	0.17	0.05	0.68[q]
	0.16[p,b], 0.018[p,d]	0.06[g]	−0.19[l], 0.56[m]
M–M (1NN/2NN)	0.11/0.04	0.05/0.03	0.34[q]
	0.17/0.09[b], 0.14/0.03[e]	0.03/0.03[g]	0.13[l], 0.08[m]
	0.2/−0.02[c], 0.075/0.035[d]		

For each item, the data on the first row are from the present calculation and others are from experiments or other calculations.
[a] Ref. [44] (Experiment, without information on the relative position of Cu atom and vacancy).
[b] Ref. [33] (First principles).
[c] Ref. [10,20] (Empirical potential).
[d] Ref. [19] (Empirical potential).
[e] Ref. [45] (First principles).
[f] Ref. [15] (Empirical potential).
[g] Ref. [16](Empirical potential, set II).
[h] Ref. [46] (Experiment).
[i] Ref. [47] (Experiment).
[j] Ref. [48] (Experiment).
[k] Ref. [49] (Experiment).
[l] Ref. [50] (First principles).
[m] Ref. [51] (Empirical potential).
[n] Ref. [52] (Empirical potential).
[o] The most stable position of a solute atom in the self-interstitial dumbbell–solute atom binding in the present calculation is the nearest neighboring lattice point parallel to the $\langle 110\rangle$ dumbbell direction for Cu and Cr [11].
[p] The most stable position of a solute atom is the nearest neighboring lattice point perpendicular to the $\langle 110\rangle$ dumbbell direction.
[q] For most stable configurations of carbon–carbon interaction and dumbbell–carbon binding, see Fig. 3.

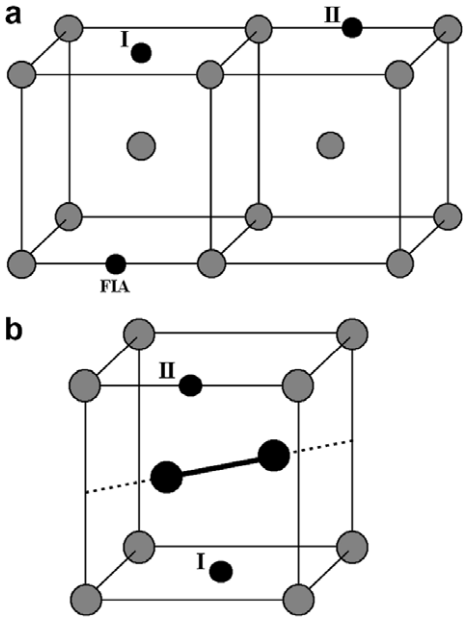

Fig. 4. The most stable configuration of (a) carbon (FIA)–carbon (I or II) interaction and (b) self-interstitial dumbbell–carbon binding, according to the present calculation (I) and a first principles calculation (II) [50]. Large and small spheres represent Fe and carbon atoms, respectively.

atoms would be present in forms of carbides and the amount of soluble carbon would be small. Alternatively, similar effect can be expected from soluble nitrogen that behaves similarly to carbon [55] and has larger solubility than carbon in bcc Fe.

The effects of solute atoms on the long-term irradiation-induced microstructure evolution can be further presumed based on the present simulation and calculation results.

With the formation of mixed dumbbells and high population of solute atoms (Cu and Cr) around interstitial dumbbells it is expected that the overall diffusivity of these solute atoms would be increased and the formation of Cu-rich or Cr-rich precipitates would be enhanced during irradiation. Such effect of Cu is expected to be much larger than that of Cr (for the same amount of solute atoms), because the binding energies between Cu atom and individual primary defects are generally higher than Cr (Table 6) and migration energy barriers of interstitial dumbbells become lower than that of self-interstitial dumbbells if Cu is involved (Table 7). On the other hands, the migration energy barriers of interstitial dumbbells increase if Cr atoms are involved, also as shown in Table 7. Therefore, it is expected the contribution from the interstitial mechanism to the overall diffusivity would be smaller in Fe–Cr alloys than in pure Fe. It should be noted here that the slowing down of single interstitial atom diffusion by the presence of Cr in Fe–Cr alloys has also been observed by a molecular dynamics simulation [56].

It is known that the void formation (nucleation) has a decisive effect on the void swelling rate [21]. Therefore, the effect of alloying elements on the void swelling can be estimated by examining the effect of solute atoms on the

Table 7
Calculated migration energy barrier of Fe–Fe self-interstitial, Fe–M and M–M dumbbells and solute atoms in bcc Fe matrix (eV)

	Fe	Fe–Cu	Fe–Cr	Fe–C
$\lvert\langle 1\,1\,0\rangle I_{Fe-M}-\langle 1\,1\,1\rangle I_{Fe-M}\rvert$	0.12	0.06	0.29	
	0.70[a], 0.73[b], 0.13[c]	0.42[b]		
$\lvert\langle 1\,1\,0\rangle I_{M-M}-\langle 1\,1\,1\rangle I_{M-M}\rvert$		0.03	0.53	
Translation-rotation jumps	0.15	0.13	0.19	
	0.34[a]			
Solute migration by vacancy mechanism	0.53	0.38	0.47	0.82
	0.55[d] , 0.55[b], 0.78[c]	0.59[b], 0.56[e]		0.81–0.88[f], 0.92[g]

The migration energy barrier for Fe, Cu and Cr is by the vacancy mechanism and that for C is by the interstitial mechanism. For each item, the data on the first row are from the present calculation and others are from experiments or other calculations.

[a] Ref. [34] (First principles).
[b] Ref. [33] (First principles).
[c] Ref. [19] (Empirical potential).
[d] Ref. [47] (Experiment).
[e] Ref. [45] (First principles).
[f] Ref. [49,53,54] (Experiment).
[g] Ref. [50] (First principles).

stability of vacancy clusters (void nuclei). The effect of solute atoms on the vacancy–vacancy binding is already presented in Table 4, which shows that the presence of any one solute atom as a nearest neighbor increases the stability (or the binding energy) of the di-vacancy cluster. The effect of Cu and Cr on the stability of void nuclei can be further clarified by calculating the binding energies between a vacancy cluster with a solute atom as a nearest neighbor and another vacancy, as a function of cluster size as shown in Fig. 5(a). Here, the binding energy of the tri-vacancy cluster means the binding energy between a di-vacancy cluster in its most stable configuration and another vacancy, and the value for the tetra-vacancy cluster means the binding energy between a tri-vacancy cluster and another vacancy, and so on. It is clearly shown that both Cu and Cr increase the stability of void nuclei and are expected to promote the void formation and thus the void swelling rate. Indeed, it has been reported [21] that the swelling rate in ferritic steels increases with increasing amount of Cr up to 10–15% above which Cr-rich precipitates form. Even though the carbon atom strongly increases the binding energy of a di-vacancy cluster, it yields a negative (−) value for the binding between a vacancy–carbon–vacancy cluster and another vacancy as shown in Fig. 5(b). The negative binding energy implies that there exists a nucleation energy barrier for void nucleation when a carbon atom presents around the void nuclei as a nearest neighbor.

In summary, increase in overall diffusivity and enhanced formation of solute-rich precipitates are expected in Fe–Cu alloys with the additional contribution from interstitial mechanism to the vacancy mechanism, during the long-term irradiation. The same is expected in Fe–Cr alloys but with less extent because of the relatively low mobility of Fe–Cr interstitial dumbbells (Table 7). However, the opposite is expected in Fe–C alloys when there remains enough amount of soluble carbon because of the strong interaction between self-interstitial dumbbells and carbon atoms and the relatively high energy barrier of carbon diffusion. With no retarding effect on the vacancy diffusion (Table 7) and increasing effect on the stability of void nuclei (Fig. 5(a)), Cu and Cr are expected to increase the void swelling rate by promoting the void nucleation. On the other hands, with strong bindings with mono- and di-vacancies and with the additional introduction of the nucleation energy barrier for void formation, soluble carbon is expected to retard the void swelling rate.

5. Conclusion

Molecular dynamics cascade simulations on pure Fe, Fe–0.5 at.% Cu, Fe–10 at.% Cr and Fe–0.1 at.% C alloys based on MEAM interatomic potentials do not show significant effects of solute elements on the number and clustering tendency of point defects such as vacancies and interstitial dumbbells. However, the effects of solute elements on the constitution of interstitial dumbbells are well observed. Based on the MD simulation results and calculated binding energies between individual defects, the effects of solute elements on the long-term irradiation-induced microstructure evolution in bcc Fe can be presumed. Cu and Cr show a strong tendency for the formation of Fe–M and M–M interstitial dumbbells. With the generally higher mobility of interstitial dumbbells compared to vacancies, it is expected that the overall diffusivity of solute atoms, Cu and Cr, would be increased, which will promote the formation of solute-rich precipitates. Such effect is expected to be small in Fe–Cr alloys because the diffusion energy barrier of Fe–Cr or Cr–Cr interstitial dumbbells is relatively high compared to that of Fe–Fe interstitial dumbbells, while the opposite is predicted for the Fe–Cu alloys. Both Cu and Cr are also expected to promote the void swelling by increasing the stability of vacancy clusters and thus enhancing the void nucleation. On the other hands, soluble carbon atom is the most slowly diffusing component in bcc Fe when compared to vacancies and interstitial dumbbells. From the strong binding between vacancies or interstitial dumbbells and carbon

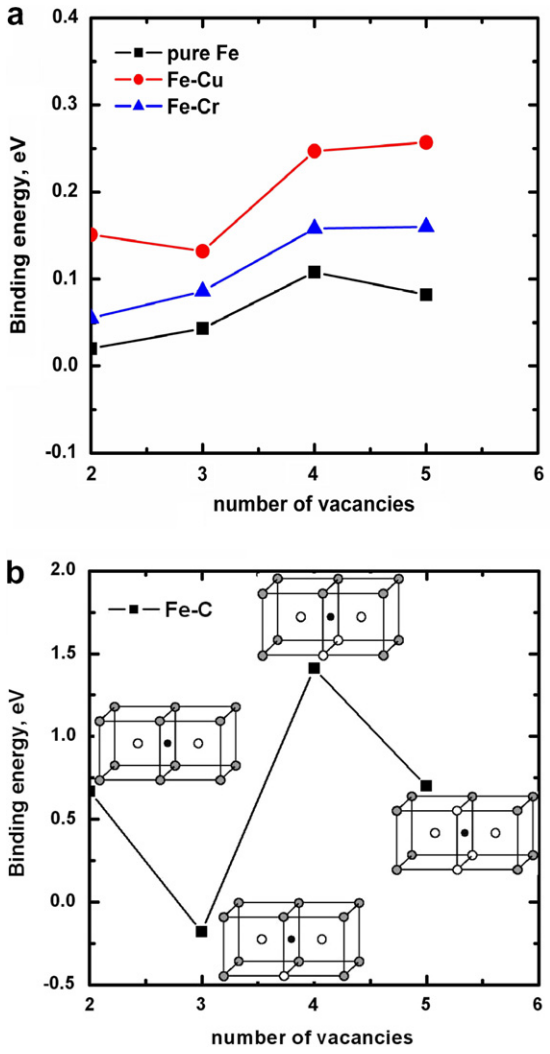

Fig. 5. Binding energy between a vacancy cluster of various size and an additional vacancy, (a) in pure Fe and when a Cu or Cr atom is located around the vacancy cluster as a nearest neighbor and (b) when a C atom is located around the vacancy cluster as a nearest neighbor. The binding energy for the tri-vacancy cluster represents the binding energy between a di-vacancy cluster in its most stable configuration and another vacancy, and so on. Most stable vacancy configurations are given for individual carbon–vacancy cluster bindings, where carbon atom and vacancies are represented by small black and empty spheres, respectively.

atoms and from the nucleation energy barrier for void formation newly exerted by the presence of carbon atoms, it is expected that soluble carbon would retard the void swelling and other irradiation-induced microstructure evolution.

Acknowledgements

This work has been financially supported by the Ministry of Science and Technology of Korea through the nuclear R&D program.

References

[1] A.F. Calder, D.J. Bacon, J. Nucl. Mater. 207 (1993) 25.
[2] R.E. Stoller, J. Nucl. Mater. 233 (1996) 999.
[3] R.E. Stoller, G.R. Odette, B.D. Wirth, J. Nucl. Mater. 251 (1997) 49.
[4] R.E. Stoller, J. Nucl. Mater. 276 (2000) 22.
[5] C.S. Becquart, C. Domain, A. Legris, J.C. Van Duysen, J. Nucl. Mater. 280 (2000) 73.
[6] R.E. Stoller, A.F. Calder, J. Nucl. Mater. 283–287 (2000) 746.
[7] Yu.N. Osetsky, D.J. Bacon, Nucl. Instrum. and Meth. B 202 (2003) 31.
[8] D.J. Bacon, Yu.N. Osetsky, R.E. Stoller, R.E. Voskoboinikov, J. Nucl. Mater. 323 (2003) 152.
[9] A.F. Calder, D.J. Bacon, in: I.M. Robertson et al. (Eds.), Microstructure Evolution During Irradiation, Mater. Res. Soc. Symp. Proc., vol. 439, Materials Research Society, Warrandale, PA, 1997, p. 521.
[10] C.S. Becquart, C. Domain, J.C. van Duysen, J.M. Raulot, J. Nucl. Mater. 294 (2001) 274.
[11] B.-J. Lee, B.D. Wirth, J.-H. Shim, J. Kwon, S.C. Kwon, J.-H. Hong, Phys. Rev. B 71 (2005) 184205.
[12] J. Wallenius, P. Olsson, C. Lagerstedt, N. Sandbers, R. Chakarova, V. Pontikis, Phys. Rev. B. 69 (2004) 094103.
[13] L. Malerba, D. Terentyev, P. Olsson, R. Chakarova, J. Wallenius, J. Nucl. Mater. 329–333 (2004) 1156.
[14] D.A. Terentyev, L. Malerba, M. Hou, Nucl. Instrum. and Meth. B 228 (2005) 156.
[15] D.A. Terentyev, L. Malerba, R. Chakarova, K. Nordlund, P. Olsson, M. Rieth, J. Wallenius, J. Nucl. Mater. 349 (2006) 119.
[16] J.-H. Shim, H.-J. Lee, Brian D. Wirth, J. Nucl. Mater. 351 (2006) 56.
[17] G.R. Odette, Scripta Metall. 11 (1983) 1183.
[18] S.G. Druce, Acta Metall. 34 (1986) 219;
P. Bowen, S.G. Druce, J.F. Knott, Acta Metall. 34 (1986) 1121.
[19] G.J. Ackland, D.J. Bacon, A.F. Calder, T. Harry, Philos. Mag. A 75 (1997) 713.
[20] M. Ludwig, D. Farkas, D. Pedraza, S. Schmauder, Model. Simul. Mater. Sci. Eng. 6 (1998) 19.
[21] F.A. Garner, M.B. Toloczko, B.H. Sencer, J. Nucl. Mater. 276 (2000) 123.
[22] R. Chakarova, V. Pontikis, J. Wallenius, Development of Fe(bcc)–Cr many body potential and cohesion model, WP6 Delivery Report Nr. 6, SPIRE project, EC contract no. FIKW-CT-2000-00058, June 2002;
P. Olsson, L. Malerba, A. Almazouzi, A first step towards a multiscale modelling of Fe–Cr alloys, SCKCEN Report, BLG-950, June 2003.
[23] B.-J. Lee, J.-H. Shim, H.M. Park, CALPHAD 25 (2001) 527.
[24] T. Takeyama, H. Takahashi, J. Phys. Soc. Jpn. 35 (1973) 939.
[25] A. Vehanen, P. Hautojarvi, J. Johansson, J. Yli-Kauppila, Phys. Rev. B 25 (1982) 2.
[26] P. Hautojarvi, L. Pollanen, A. Vehanen, J. Yli-Kauppila, J. Nucl. Mater. 114 (1983) 250.
[27] B.-J. Lee, Acta Mater. 54 (2006) 701.
[28] B.-J. Lee, M.I. Baskes, Phys. Rev. B 62 (2000) 8564.
[29] B.-J. Lee, M.I. Baskes, H. Kim, Y.K. Cho, Phys. Rev. B 64 (2001) 184102.
[30] M.I. Baskes, Phys. Rev. B 46 (1992) 2727.
[31] M. Parrinello, A. Rahman, Phys. Rev. Lett. 45 (1980) 1196;
M. Parrinello, A. Rahman, J. Appl. Phys. 52 (1981) 7182;
M. Parrinello, A. Rahman, J. Chem. Phys. 76 (1982) 2662.
[32] L. Verlet, Phys. Rev. 159 (1967) 98;
L. Verlet, Phys. Rev. 165 (1967) 201.
[33] C. Domain, C.S. Becquart, Phys. Rev. B 65 (2001) 024103.
[34] C.-C. Fu, F. Willaime, Phys. Rev. Lett. 92 (2004) 175503;
C.-C. Fu, F. Willaime, Phys. Rev. B 72 (2005) 064117.
[35] W.A. Dench, Faraday Soc. Trans. 59 (1963) 1279.
[36] P. Olsson, J. Wallenius, C. Domain, K. Nordlund, L. Malerba, Phys. Rev. B. 72 (2005) 214119.
[37] J. Wallenius, P. Olsson, L. Malerba, D. Terentyev, Nucl. Instrum. and Meth. B 255 (2007) 68.
[38] I. Ansara, and Å. Jansson, Trita-Mac-0533, KTH, Stockholm, 1993.
[39] J.-O. Andersson, B. Sundman, CALPHAD 11 (1987) 83.

[40] F. Maury, A. Lucasson, P. Lucasson, P. Moser, F. Faudot, J. Phys.: Condens. Matter 2 (1990) 9291.
[41] A.L. Nikolaev, V.L. Arbuzov, A.E. Davletshin, J. Phys.: Condens. Matter 9 (1997) 4385.
[42] H. Abe, E. Kuramoto, J. Nucl. Mater. 271&272 (1999) 209.
[43] A.L. Nikolaev, J. Phys.: Condens. Matter 11 (1999) 8633.
[44] G. Brauer, K. Popp, Phys. Status Solidi B 102 (1987) 79.
[45] E. Vincent, C.S. Becquart, C. Domain, Nucl. Instrum. and Meth. B 228 (2005) 137.
[46] R.A. Arndt, A.C. Damask, Acta Metall. 12 (1964) 341.
[47] A. Vehanen, P. Hautojärvi, J. Johansson, J. Yli-Kauppila, P. Moser, Phys. Rev. B 25 (1982) 762.
[48] M. Weller, J. Diehl, Scripta Metall. 10 (1976) 101.
[49] S. Takaki, J. Fuss, H. Kugler, U. Dedek, H. Schults, Radiat. Eff. 79 (1983) 87.
[50] C. Domain, C.S. Becquart, J. Foct, Phys. Rev. B. 69 (2004) 144112.
[51] R.A. Johnson, G.J. Dienes, A.C. Damask, Acta Metall. 12 (1964) 1215.
[52] V. Rosato, Acta Metall. 37 (1989) 2759.
[53] J. Askill, Tracer Diffusion Data for Metals, Alloys and Simple Oxides, Plenum, New York, 1970.
[54] A.D. Le Claire, in: H. Mehrer (Ed.), Numerical data and functional relationships in science and technology, Landolt-Börnstein, New Series, Group III, vol. 26, Springer-Verlag, Berlin, 1990, p. 480, Chapter 8.
[55] B.-J. Lee, T.-H. Lee, S.-J. Kim, Acta Mater. 54 (2006) 4597.
[56] D. Terentyev, L. Malerba, J. Nucl. Mater. 329–333 (2004) 1161.